Millimeter Wave MISO-OFDM Transmissions in an Intra-Wagon Environment

Concepción Sanchis Borras[1], José-María Molina-García-Pardo[2], Lorenzo Rubio[3], *Senior Member, IEEE*, Juan Pascual García[2], Vicent M. Rodrigo Peñarrocha[3], Leandro J. Llacer[2], *Senior Member, IEEE*, and Juan Reig[3], *Senior Member, IEEE*.

Abstract— In this paper, the maximum achievable throughput is analyzed in the intra-wagon channel when multiple-input single-output (MISO) and orthogonal frequency division multiplexing (OFDM), MISO-OFDM, techniques are used. This analysis is performed from real wideband propagation channel measurements at 28 and 37 GHz, two potential frequency bands to deploy the future fifth-generation (5G) wireless communications networks. Four different scenarios in terms of the access point (AP) and user equipment (UE) positions inside the wagon have been considered, using 4 and 8 antennas at the AP. The performance of both quasi-orthogonal space-time block code (QSTBC), combined with Hadamard matrices, and transmit beamforming techniques is studied and evaluated from simulation results. The simulation results take into account the signal-to-noise ratio (SNR) and the antenna correlation for each antenna array configuration at the AP. These results provide useful insight to better understand the intra-wagon channel properties and deploy the future 5G wireless networks in this particular scenario at mmWave frequencies, where high-data-rates are expected to support different types of digital applications.

Index Terms—MISO-OFDM, mmWave, 28 GHz, 37 GHz, Intra-wagon communication, 5G.

I. INTRODUCTION

Contemporary rail transportation models have shifted to green communication methods, which are more energy efficient, less expensive and have a smaller environment impact than other transport models [1]. Rail traffic communications are expected to be seamless and wireless with a throughput of several gigabits [2]. Remaining connected while one is on the move is the desire of passengers, because they can spend their time for working, access to different types of digital information, enjoying multimedia applications, and entertainment, among others.

C. Sanchis Borras is affiliated to the Department of Technical Sciences, Universidad Católica San Antonio de Murcia (UCAM), 30107 Murcia, Spain (e-mail: csanchis@ucam.edu).

J.M. Molina-Garcia-Pardo, L. Juan Llacer and Juan Pascual-Garcia are affiliated to the Information Technologies and Communications Department, Universidad Politécnica de Cartagena, Cartagena 30202, Spain (email: {josemaria.molina;juan.pascual;leandro.juan}@upct.es).

L. Rubio, V. M. Rodrigo and J. Reig are with the iTEAM Research Institute, at the Universitat Politècnica de València, Valencia 46022, Spain (email:{lrubio; vrodrigo; jreigp}@dcom.upv.es).

In this context, millimeter wave (mmWave) is a promising new technology capable of providing high bandwidths to support the aforementioned applications through the future fifth-generation (5G) wireless communications and beyond 5G [3], [4]. Although the mmWave corresponds to the frequencies between 30 and 300 GHz, the 10-30 GHz frequency band is sometimes included by the industry in the mmWave frequencies [5]. In general, the propagation characteristics in mmWave are different from sub-6 GHz frequency bands. MmWave bands suffer high path loss, higher penetration losses, etc. In certain environments, such as inside intra-wagons, some of these effects can increase, thus conditioning the propagation and the final performance of wireless networks. Therefore, a proper propagation and throughput analysis is essential to the deployment of the future wireless networks in these particular environments and frequencies.

In USA, the 28 GHz (27.5-28.35 GHz) and 37 GHz (37-40 GHz) frequency bands were licensed for the deployment the future 5G mmWave communications, while both China and the European Union have chosen the 26 GHz (24.25-27.5 GHz) frequency band. These frequency bands are in accordance with the World Radio Communication Conference (WRC) of the International Telecommunication Union (ITU), held in 2019 [6].

In [2] at least five future scenarios related to railway service communications have been defined: train-to-infrastructure, inter-wagon, intra-wagon, inside-the-station and infrastructure-to-infrastructure scenarios. In the existing research, most of the efforts have been made on the analysis of the propagation channel based on measurement data and simulations. In [7], the authors analyze the throughput of the data link inside train communications using intelligent transportation systems (ITS) measurement data at 5 GHz (ITS-G5). In [8], a ray-tracing tool was used to simulate and analyze the propagation channel conditions at 29.5 GHz. In addition, a 3D ray tracer was employed in [9] to investigate several propagation parameters at 25.25 GHz in a train-to-infrastructure scenario. Wideband channel measurements were collected at 60 GHz in a train-to-infrastructure scenario in [10]. Also, in [11] the influence of typical railway objects in a mmWave propagation channel is analyzed for train-to-infrastructure and intra-wagon scenarios with various configurations. In [12], [13] some propagation results were derived from channel

measurements in an intra-wagon environment in the 26.6-40 GHz and 25-40 GHz frequency ranges, respectively. While in [14] the intra-wagon channel at 60 and 300 GHz bands are characterized through ray-tracing simulations validated from the measurement data.

Together with mmWave, massive multiple-input multiple-output (mMIMO) techniques are considerably relevant in the context of 5G wireless communications in intra-wagon environments in order to provide the expected high-data-rate in real-time. Space-time block code (STBC) techniques can achieve these data-rates with minimum bit error rate (BER). The applicability of quasi-orthogonal STBC (QSTBC) in mMIMO has been analyzed in [15], and the performance of QSTBC algorithms in mmWave at the 94 GHz in indoor environments has been studied in [16]. It has also been demonstrated that QSTBC techniques can be applied in mMIMO [17] together with beamforming techniques achieving full transmission rate for any number of transmit antennas. On the other hand, it is known that in mmWave mMIMO systems hybrid analog and digital beamforming (HBF) based techniques are used to mitigate the effect of the propagation loss and the hardware cost and power consumption [18].

In order to design and deploy the future 5G intra-wagon mmWave networks, it is necessary to analyze the performance of the data link in this particular scenario. The intra-wagon scenario describes the link between access points (APs) and the user equipment (UE) inside a wagon. To increase the data-rate, the wireless network can take advantage of massive antennas placed at the AP. Thus, it is of interest to analyze the throughput of a complete multiple-input single-input (MISO) orthogonal frequency division multiplexing (OFDM) link, a MIMO-OFDM link, in intra-wagon communications.

To the best of the authors' knowledge, there are no experimental studies on the mmWave MIMO throughput in an intra-wagon scenario. For this reason, in this paper, from wideband channel measurements in the 25-40 GHz frequency range, the achievable throughput is analyzed when MISO-OFDM techniques are used. Four different scenarios inside a wagon, in terms of the positions of the AP and UE, have been considered. The throughput in all scenarios has been analyzed considering 4 and 8 antennas at the AP. Two algorithms to improve the BER have been evaluated. On the one hand, the performance of the QSTBC combined with Hadamard matrices (HQSTBC) [15] are evaluated from simulation results. On the other hand, the transmit beamforming technique based on channel phase equalization [19] has been studied. The authors have chosen these algorithms because these are common and simple techniques to implement in MIMO systems. In future works more complex techniques mentioned above [17], [18], will be applied in mMIMO systems, which will be compared with the ones used in the present paper.

The paper is organized as follows. Section II describes the intra-wagon environment and the propagation setup used in the channel measurements. Section III describes the methodology followed, the algorithms implemented, the antenna array configurations at the AP and physical layer parameters, to obtain the simulation results. Signal-to-noise ratio (SNR), antenna correlation properties at the AP and the achievable throughput are presented and discussed in Section IV. Finally, the conclusions are presented in Section V.

II. Measurement Campaign

A. Propagation environment

The measurement campaign was carried out inside a metro train convoy of Ferrocarriles de la Generalitat Valenciana (FGV) in Valencia, Spain. The union of four wagons, defining a single space, forms the convoy. The interior dimensions of the convoy are 55.25 m (length) by 2.55 m (width) by 2.15 m (high). The convoy has a small cabin for the driver on both ends

There are many handholds and seats for passengers. The seats are resin molded, reinforced with glass fiber. The handholds and the roof are made of stainless steel, windows are made of laminated glass, and the doors are of aluminum and glass. This environment is characterized by the presence of numerous metallic elements, which causes a rich-multipath propagation that can decrease the spatial correlation [20]. Fig. 1 shows the interior view of the convoy.

B. Measurement Setup

Complex channel transfer functions (CTF) have been measured in the frequency domain using a channel sounder based on the Keysight PNA N5227 vector network analyzer (VNA). This channel sounder has been calibrated and validated in other scenarios [16], [21]. The Q-PAR QOM-SL-0.8-40-K-SG-L ultra-wideband omnidirectional antennas have been used at the transmitter (Tx) and receiver (Rx) ends. These antennas have vertical polarization and omnidirectional radiation pattern in the horizontal plane. The Tx subsystem was connected to the VNA through a broadband radio over fiber (RoF) link to avoid the high losses of cables at mmWave frequencies, thus increasing both the dynamic range in the measurements and the Tx-Rx distance.

The Rx antenna was located in an XY positioning system, implementing a 7×7 virtual uniform rectangular array (URA). Thus, 49 (7×7) CTFs have been measured for each Tx position. A personal computer controlled both the VNA and the XY positioning system, measuring the $S_{21}(f)$ scattering parameter directly from 25 to 40 GHz, equivalent to the CTF of the propagation channel [22]. The separation of the URA elements has been 3.04 mm, less than $\lambda/2 = 3.7$ mm at 40 GHz. Measuring in this frequency range has the advantage of being able to analyze and compare the behavior of the propagation channel at the 28 and 37 GHz bands in the same propagation conditions. A response calibration of the channel sounder has been carried out prior to the

measurements, with the exception of the antennas. Thus, the measured CTF takes into account the radio channel [23].

The $S_{21}(f)$ scattering parameter has been measured using 8192 frequency points, avoiding temporal aliasing. The frequency resolution is about 1.83 MHz, which corresponds to a maximum observable distance of 164 m, larger than the convoy dimensions. The bandwidth of the intermediate frequency filter at the VNA was set to 100 Hz. This value guarantees a good trade-off between dynamic range and acquisition time in the measurement.

Fig. 1. Interior of the metro train.

The Tx antenna has been manually placed in different locations along the convoy, imitating the position of a UE. The URA has been placed in two different positions imitating the position of an AP that serves the passengers inside the convoy. The acquisition time was about 2 hours per Tx position. To guarantee stationary channel conditions, the convoy was parked away from other convoys and staff, and the doors remained closed to prevent people from entering during the measurements.

The channel measurements have been collected in line-of-sight (LOS) conditions. The Rx antenna height was 1.63 m with respect to the floor level. Based on the Tx and URA locations, four scenarios have been defined (see Fig. 2):

Scenario 1: The URA was placed next to the cabin (2 m from the cabin), whereas the Tx antenna was placed in the central position of the corridor at a height of 1.45 m. This scenario corresponds to the situation in which a passenger travels standing. Eight Tx locations were measured. The cabin-Tx distance in this scenario, denoted by d, is $d = \{7, 12, 17, 22, 37, 42, 47, 52\}$ m.

Scenario 2: The URA was placed next to the cabin (2 m from the cabin), whereas the Tx antenna was placed close to the seats at a height of 0.85 m. This scenario corresponds to the situation in which a passenger travels seated. Six Tx locations were measured. The cabin-Tx distance in this scenario is $d = \{7, 14, 22, 42, 47, 52\}$ m.

Scenario 3: The URA was placed in the middle of the convoy (19.5 m from the cabin), whereas the Tx antenna was placed in the central position of the corridor at a height of 1.45 m. Four Tx locations were measured. The cabin-Tx distance in this scenario is $d = \{5.5, 14.5, 24.5, 33.5\}$ m.

Scenario 4: The URA was placed in the middle of the convoy (19.5 m from the cabin), whereas the Tx antenna was placed close to the seats at a height of 0.85 m. Four Tx locations were measured. The cabin-Tx distance in this scenario is $d = \{9.5, 14.5, 24.5, 29.5\}$ m.

The propagation channel is assumed bidirectional. For this reason, during the measurements it has been considered that the UE transmit and AP receive. It is important to note that Scenarios 1 and 3 correspond to the situation in which the UE travels standing, therefore the TX antenna is at a height of 1.45 m, while in Scenarios 2 and 4 the TX antenna is at 0.85 m simulating a seated UE. More details about the channel measurement campaign can be found in [13], where a path loss and time-dispersion analysis was made.
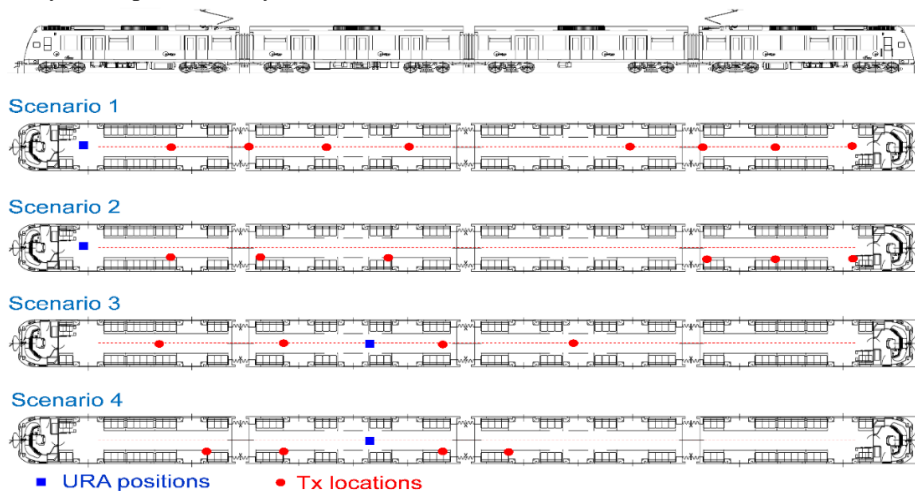

Scenario 1

Scenario 2

Scenario 3

Scenario 4

■ URA positions   ● Tx locations

Fig. 2. Locations of Rx and Tx in the four scenarios.

III. METHODOLOGY

In all the scenarios described above measurements were acquired with URA-Rx fixed in one position and Tx moving along the wagon for reducing the complexity and difficulty of the measurements acquisition. In addition, the Tx acted as the UE and the Rx as the AP.

The idea is to apply MISO techniques increasing the complexity of the AP and simplifying the UE by using a single antenna. For this purpose, evoking the channel reciprocity principle [22] by which the channel characteristics, e.g. path loss and channel correlation, are the same in uplink and downlink, the channel measurements can be used to analyze the MISO link between the AP and the UE (AP → UE).

This section presents the two algorithms considered in the simulation performance, describes the antennas configuration at the AP, and summarizes the parameters of the physical layer used in the throughput simulation.

A. Implemented Algorithms

Two common algorithms have been simulated to study their application in intra-wagon environments.

QSTBC algorithm, lacks of orthogonality causes inter symbol interference (ISI) in the decoding matrix and worsens the BER. Therefore, QSTBC combined with Hadamard matrices (HQSTBC) [15], which improves the BER, has been selected.

On the other hand, a simple transmit beamforming (T-BF) technique based on channel phase equalization has been simulated [19]. This technique is implemented at the AP and channel estimation is required. In addition, it facilitates decoding at the UE.

1) Hadamard quasi-orthogonal space-time block code

The received symbols at the receiver applying the HQSTBC algorithm can be represented as follows:

$$x = H_{\text{new}} s + n , \tag{1}$$

where $s = [s_1 \, s_2 \, ... \, s_{Nt}]$ represents the symbols transmitted by the N_t antennas at the AP, n is additive white gaussian noise (AWGN) and H_{new} is calculated as:

$$H_{\text{new}} = H_{N_t} \times M_{N_t} , \tag{2}$$

where M_{Nt} is the Hadamard matrix, which in the four- and eight-antenna cases is given by:

$$M_4 = \begin{bmatrix} 1 & 1 & 1 & 1 \\ 1 & -1 & 1 & -1 \\ 1 & 1 & -1 & -1 \\ 1 & -1 & -1 & 1 \end{bmatrix} \tag{3}$$

$$M_8 = \begin{bmatrix} 1 & 1 & 1 & 1 & 1 & 1 & 1 & 1 \\ 1 & -1 & 1 & -1 & 1 & -1 & 1 & -1 \\ 1 & 1 & -1 & -1 & 1 & 1 & -1 & -1 \\ 1 & -1 & -1 & 1 & 1 & -1 & -1 & 1 \\ 1 & 1 & 1 & 1 & -1 & -1 & -1 & -1 \\ 1 & -1 & 1 & -1 & -1 & 1 & -1 & 1 \\ 1 & 1 & -1 & -1 & -1 & -1 & 1 & 1 \\ 1 & -1 & -1 & 1 & -1 & 1 & 1 & -1 \end{bmatrix} \tag{4}$$

and H_{Nt} is the space-time code matrix, which in the four- and eight-antenna cases is defined as follows:

$$H_4 = \begin{bmatrix} h_1 & h_2 & h_3 & h_4 \\ h_2^* & -h_1^* & h_4^* & -h_3^* \\ h_3 & h_4 & h_1 & h_2 \\ h_4^* & -h_3^* & h_2^* & -h_1^* \end{bmatrix} \tag{5}$$

$$H_8 = \begin{bmatrix} h_1 & h_2 & h_3 & h_4 & h_5 & h_6 & h_7 & h_8 \\ h_2^* & -h_1^* & h_4^* & -h_3^* & h_6^* & -h_5^* & h_8^* & -h_7^* \\ h_3 & h_4 & h_1 & h_2 & h_7 & h_8 & h_5 & h_6 \\ h_4^* & -h_3^* & h_2^* & -h_1^* & h_8^* & -h_7^* & h_6^* & -h_5^* \\ h_5 & h_6 & h_7 & h_8 & h_1 & h_2 & h_3 & h_4 \\ h_6^* & -h_5^* & h_8^* & -h_7^* & h_2^* & -h_1^* & h_4^* & -h_3^* \\ h_7 & h_8 & h_5 & h_6 & h_3 & h_4 & h_1 & h_2 \\ h_8^* & -h_7^* & h_6^* & -h_5^* & h_4^* & -h_3^* & h_2^* & -h_1^* \end{bmatrix} \tag{6}$$

where h_i is the channel response in the frequency domain associated with the antenna i, and * represents the complex conjugate.

The pairs of antennas whose coding is quasi-orthogonal are (1-3) and (2-4) in the case of four antennas and (1-3), (1-5), (1-7), (2-4), (2-6), (2-8), (3-5), (3-7), (4-6), (4-8), (5-7) and (6-8) in the case eight antennas.

At the receiver linear decoding method is applied utilizing Zero-Forcing (ZF) [15]. The estimation of the received symbols is obtained as:

$$\hat{s} = H_{\text{new}}{}^{\mathcal{H}} H_{\text{new}} s + H_{\text{new}}{}^{\mathcal{H}} n , \tag{7}$$

where $(\cdot)^{\mathcal{H}}$ represents the conjugate transpose of $(\cdot)$.

2) Transmit beamforming

The same information is sent from each antenna at the AP, multiplied by a phase factor equivalent to the inverse of the channel phase associated with each of AP antenna.

$$x = \begin{bmatrix} h_1 h_2 \dots h_{N_t} \end{bmatrix} \begin{bmatrix} exp(-j\theta_1) \\ exp(-j\theta_2) \\ \vdots \\ exp(-j\theta_{N_t}) \end{bmatrix} \begin{bmatrix} s_1 \\ s_1 \\ \vdots \\ s_1 \end{bmatrix} + n \, , \qquad (8)$$

where $h_i = |h_i| exp(j\theta_i)$.

Thus, the signals transmitted by each antenna are added coherently at the UE antenna as:

$$x = \left(|h_1| + |h_2| + \cdots + |h_{N_t}| \right)s_1 + n \qquad (9)$$

Finally, the received symbol is estimated as:

$$\hat{s}_1 = \frac{x}{\left(|h_1| + |h_2| + \cdots + |h_{N_t}| \right)} \qquad (10)$$

B. Antenna Array Configurations

The performance of a MISO-OFDM system is studied when the AP has multiples antennas. Based on the channel measurements and the URA geometry, 4 and 8 antennas at the AP are considered. Note that in the HQSTBC algorithm the number of antennas must be a power of two. The configurations with the lowest correlations between transmitting antennas were chosen from the measurements.

Fig. 3 shows the four- and eight-antenna configurations selected from the transmitting 7x7 URA. The locations of the four or eight AP antennas are marked in orange. The numbering indicates the distribution of the antennas. This distribution is important when the HQSTBC algorithm is applied, since the coding is quasi-orthogonal between certain pairs of antennas, as discussed above. The chosen numbering is the one that maximizes the distance between antennas whose coding is quasi-orthogonal.
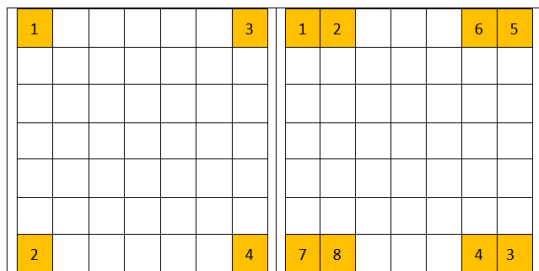

Fig. 3. Transmitter system configurations

C. Physical Layer Parameters

In the failure to define the frequency bands in mmWave and to complete the 5G specifications, the specifications of the 802.15.3c standard [24] have been chosen as reference in our work.

Table I summarizes the physical layer specifications applied. The modulation schemes studied were 64 quadrature amplitude modulation (64 QAM) and 16 QAM. The forward error correction (FEC) technique is based on structured soft-decision low density parity

check (LDPC) codes and the coding rates were 1/2, 3/4 and 5/8. The MISO techniques simulated were HQSTBC and phase equalization of the channel (transmit beamforming). Finally, OFDM symbols were transmitted via 512 subcarriers, including 371 occupied subcarriers with a separation of 5.15 MHz occupying a bandwidth of 2 GHz. Interpolation has been used to derive the frequency points described in the standard out of the 8192 reference points obtained in the measurement campaign.

Table II shows the bit rate (R_b) corresponding to each of the modulation and coding schemes (MCS). It is important to note that the bit rate is the same for all MISO techniques implemented.

TABLE I
SYSTEM PARAMETERS FROM THE IEEE802.15.3C STANDARD FOR THROUGHPUT EVALUATION

Parameter	Value
Sampling rate	2640 MHz
FFT points	512
Occupied subcarriers (Inc. DC subcarrier)	371
Modulation type	16 QAM, 64 QAM
Forward error correction	Structured LDPC
Coding rate	1/2, 3/4, 5/8

TABLE II
BIT RATE FOR EACH MODULATION AND CODING SCHEME USED

MCS	Coding rate modulation	Bit rate(Gbps)
4	1/2 16 QAM	3.08
5	3/4 16 QAM	4.62
7	5/8 64 QAM	5.77

IV. RESULTS AND DISCUSSION

This section presents firstly physical layer results such as SNR (Subsection III-A) and correlation (Subsection III-B), which are needed to understand the throughout analysis. Then, Subsection III-C shows the performance of the MISO algorithms in each scenario.

It is noteworthy to mention that the following tables and figures show the different positions measured as the distance between the train cab and UE, rather than the distance between the AP and UE. This has been decided because in Scenarios 3 and 4 (where AP is in the middle of the wagon) if the AP/UE distance is selected, all positions could not be represented because there are positions where the AP/UE distance coincides in the same scenario (see Fig. 2).

A. Signal-to-noise ratio

The signal-to-noise ratio (SNR) measures the difference between the signal and the noise in logarithmic units. The path loss (L) is computed by the measurements in the wagon, the noise is assumed as AWGN, and the equivalent isotopically radiated power (EIRP) is adjusted

so as we have a limiting situation of SNR = 5 dB in the worst case ($SNR_{\min}$). This is the same approach followed in [16].

The worst case is obtained at 37 GHz in the scenario 2, at 47 m, where the losses can be named $L_{47m,Sce.2,37GHz}$. Then the reference *EIRP* can be obtained by:

$$EIRP_{ref} = SNR_{\min} + L_{47m,Sce.2,37GHz} - G_r + P_n , \qquad (11)$$

where G_r is the receiving antenna gain and P_n is the AWGN for this system (-79.4 dBm). The reason of fixing 5 dB of $SNR_{\min}$ was to allow observation of variations in the throughput, since no errors occurred at larger SNRs. The calculated $EIRP_{ref}$ is 0 dBm, in our case. Then, for any position, the *SNR* is computed as:

$$SNR = EIPR_{ref} - L + G_r - P_n \qquad (12)$$

At each distance, the SNR was averaged across the 371 frequencies and 49 combinations (7x7x1). Fig. 4 shows the average SNR at 28 GHz and 37 GHz for each distance, and for the four scenarios under studied. Recall that in scenario 1 and 2 the AP is at one ends of the wagon (2 m from the train cabin), while in 3 and 4 are in the middle (29.5 m from the train cabin).
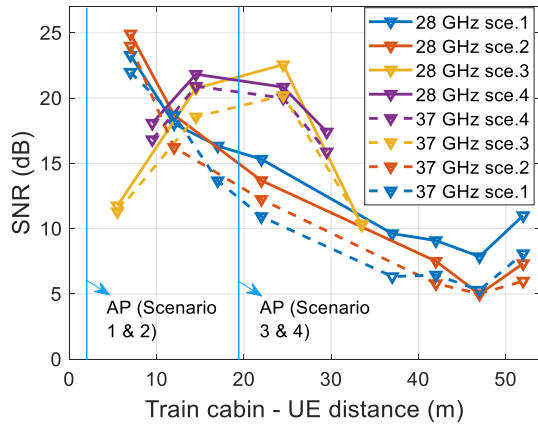

Fig. 4. SNR (dB) as a function of the Train cabin-UE distance for the four scenarios and both the bands 28 and 37 GHz

The SNR was higher at the 28 GHz band. Since the same EIRP was applied to both regardless of whether the AP was at the end (scenarios 1 and 2) or in the middle of the wagon (scenarios 3 and 4), one can see that, for distances of 14 m upwards, the SNR was higher in Scenarios 3 and 4 than in Scenarios 1 and 2. This is because the maximum AP/UE distance is higher when the AP was at the end of the wagon (Scenarios 1 and 2), causing higher propagation losses. For instance, at 29.5 m SNRs of 17.4, 16.5, 12 and 11 dB were observed in Scenarios 4, 3, 1 and 2, respectively. It is worth noting that for train cabin-UE distances larger than 50 m in scenarios 1 and 2, the SNR increases due to the existence

of a waveguide effect as a consequence of the elongated structure of the environment [13].

Finally, in scenarios 3 and 4 the highest SNR was reached in the distance range between 14 - 25 m instead of the < 10 m distance range, because the AP/UE separation is smaller in the 14 - 25 m distance range.

B. Correlation Properties at the AP

Correlation measures the similarity of two or more channel transfer functions (CTFs), and it is the key point of multiantenna systems. Here, MISO matrices are studied, so correlation is measured in the URA side.

The channel matrix *H* is defined as follows:

$$H = (h^1 \; h^2 \; h^3 \; h^4) , \qquad (13)$$

where $h^i = [h_1^i \; h_2^i \; ... \; h_{371}^i]^T$ is the column vector that represents the channel response associated with the transmitting antenna *i* for each frequency of the band studied (from 1 to 371 frequencies which corresponds to the sampled system bandwidth).

The correlation matrix is calculated using the Pearson coefficient [25]:

$$\rho_{pq} = \frac{E[h^p \cdot h^{q*}]}{\sqrt{E[|h^p|^2] \cdot E[|h^q|^2]}} \; \text{ with } p \neq q , \qquad (14)$$

where E [] is the expectation operator and h^p and h^q are the *p* and *q* columns of the channel matrix *H,* respectively. Finally, the mean correlation between the transmitting antenna elements was computed as the average of the non-one coefficients $\rho_{p,q}$.

a)

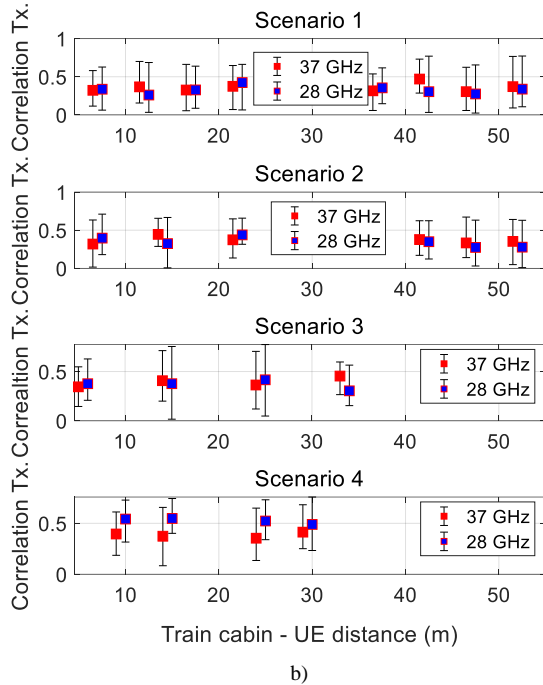mean correlation is 0.41 and 0.26 at 28 GHz and 37 GHz, respectively.
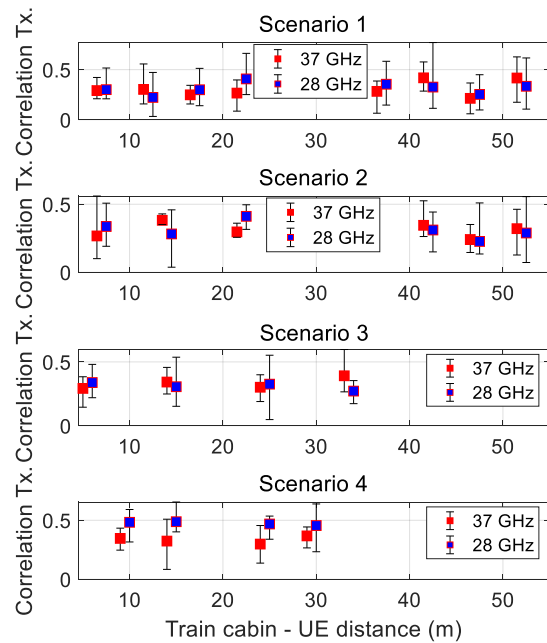
Fig. 5. AP mean correlations and confidence interval (by both band and antenna configuration) for a) 4 antenna elements; b) 8 antenna elements

Fig. 5 shows the AP correlation obtained at each distance by both band and antenna configuration. The four-antenna configuration provided lower correlations due to the larger electrical separation.

For sake of clarity, Tables III and IV describe in more detail the mean correlation obtained in these configurations at the 28 GHz and 37 GHz frequency bands, in each of the 4 situations described previously. It is important to note that the measured points in each scenario are not exactly the same in some cases. Hence, values associated with the same or similar distances should be compared in the analysis of correlations. In the 28 GHz band, lower correlations were found in the standing scenarios (Scenarios 1 and 3). Especially, using 8 antennas it can be observed in the Table III that Scenario 1 presents lower correlations than Scenario 2. For example, the mean correlation at a distance of 7 m is 0.33 and 0.40 in the Scenario 1 and 2, respectively, being lower in Scenario 1. On the other hand, at a distance of 14.5 m the mean correlation is 0.37 and 0.54 in the Scenario 3 and 4, respectively, being lower in Scenario 3. However, at 37 GHz lower correlations were obtained in Scenario 1 and 4. For instance, using 8 antennas at a distance of 14.5 m the mean correlation is 0.40 and 0.37 in the Scenario 3 and 4, respectively, being smaller in Scenario 4. In addition, at 37 GHz in Scenario 1 the correlations are lower than the other scenarios for distances up to 37 m.

If both bands are compared, at 37 GHz lower correlations are obtained, in general. For example, in Scenario 1 using 4 antennas at a distance of 22 m the

TABLE III
MEAN CORRELATIONS AT THE AP IN THE FOUR SCENARIOS AT 28 GHZ

	Scenario 1		Scenario 2		Scenario 3		Scenario 4	
d (m)	4	8	4	8	4	8	4	8
5.5					0.33	0.37		
7	0.30	0.33	0.33	0.40				
9.5							0.48	0.54
12	0.22	0.26						
14			0.28	0.32				
14.5					0.30	0.37	0.48	0.54
17	0.29	0.32						
22	0.41	0.42	0.41	0.44				
24.5					0.32	0.41	0.46	0.52
29.5							0.45	0.48
33.5					0.27	0.30		
37	0.35	0.35						
42	0.32	0.30	0.31	0.35				
47	0.25	0.27	0.23	0.27				
52	0.33	0.33	0.29	0.28				

TABLE IV
MEAN CORRELATIONS AT THE AP IN THE FOUR SCENARIOS AT 37 GHZ

	Scenario 1		Scenario 2		Scenario 3		Scenario 4	
d(m)	4	8	4	8	4	8	4	8
5.5					0.29	0.34		
7	0.29	0.32	0.27	0.32				
9.5							0.34	0.39
12	0.30	0.36						
14			0.38	0.44				
14.5					0.34	0.40	0.32	0.37
17	0.25	0.33						
22	0.26	0.37	0.29	0.37				
24.5					0.30	0.36	0.29	0.35
29.5							0.36	0.41
33.5					0.39	0.45		
37	0.28	0.31						
42	0.42	0.47	0.34	0.38				
47	0.21	0.30	0.24	0.33				
52	0.38	0.37	0.32	0.35				

Finally, since the HQSTBC algorithm uses quasi-orthogonal space-time codes, it is influenced by the correlation between pairs of antennas whose coding is quasi-orthogonal, as mentioned above. Therefore, in order to explain the behavior of the HQSTBC algorithm better, we include the Table V. It shows at 28 GHz the mean correlation between the antennas (1-3) and (2-4) in the four-antennas case and between the antennas (1-3), (1-5), (1-7), (2-4), (2-6), (2-8), (3-5), (3-7), (4-6), (4-8), (5-7) and (6-8) in the eight-antennas case. The correlation coefficients for each frequency are calculated using (3) and then averaged. In this case, the channel matrix H necessary to calculate those correlation coefficients is the space-time code matrix, which in the four- and eight-antenna cases is given by (5) and (6).

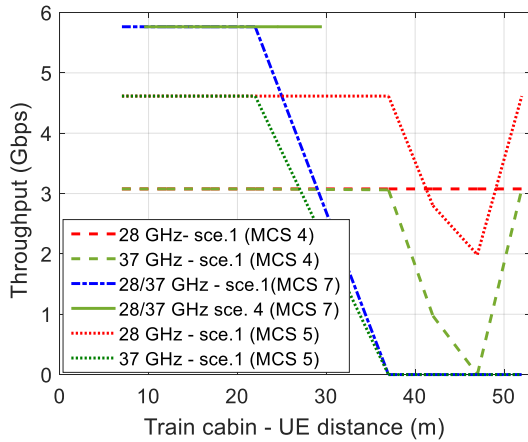| d(m)	Scenario 1		Scenario 2		Scenario 3		Scenario 4	
	4	8	4	8	4	8	4	8
5.5					0.49	0.27		
7	0.48	0.32	0.44	0.24				
9.5							0.50	0.21
12	0.47	0.34						
14			0.47	0.33				
14.5					0.51	0.17	0.57	0.20
17	0.50	0.35						
22	0.44	0.38	0.37	0.29				
24.5					0.47	0.19	0.36	0.21
29.5							0.41	0.21
33.5					0.38	0.29		
37	0.42	0.34						
42	0.41	0.42	0.39	0.30				
47	0.38	0.36	0.35	0.34				
52	0.44	0.36	0.38	0.37				

Fig. 6. Best throughput at the 28 and 37 GHz bands (Scenarios 1 and 4)

C. Throughput Analysis

In this sub-section, the performance will be studied in terms of the throughput. The simulated models were implemented with the Matlab software using the Monte Carlo method. In order to calculate the Packet Error Rate (PER), we first simulated 100 000 packets per position, to obtain a minimum PER of 10^{-3}, which is sufficiently low to allow comparison of the different algorithms. The simulations use the CTF measured experimentally as described in Section II. In addition, as was explained in Section III.C, it has been interpolated to adjust the frequency points to the points included in the standard. Finally, throughput was calculated using the PER as $R_b(1 - \text{PER})$, where R_b is the physical layer bit rate shown in Table II [26].

1) Performance According to Scenario and Band

Fig. 6 shows the best results obtained in both the 28 GHz and 37 GHz bands. Accordingly, it shows the Scenarios 1 and 4, using the transmit beamforming

algorithm with 8 antennas. With the AP at the end of the wagon (Scenario 1) applying the MCS 4 (3.08 Gbps) and MCS 5 (4.62 Gbps) schemes yielded maximum distances of 52 and 37 m respectively in the 28 GHz band, whereas in the 37 GHz band the corresponding maximum distances were 37 and 22 m. This can be explained due to in all scenarios the SNR applied is higher at 28 GHz, as shown the Fig. 4. However, when applying the scheme MCS 7 to both the 28 GHz and 37 GHz bands the maximum throughput reached is 5.7 Gbps at distances of up to 22 m. This is because the minimum SNR needed is higher, since the modulation used in this scheme was 64 QAM (see Table II). On the other hand, when the AP was in the middle wagon (Scenario 4) the maximum throughput (5.7 Gbps) was achieved at distances of up to 29.5 m in both the 28 GHz and 37 GHz bands.

Scenario	MCS	MISO algorithm	Max. train cabin - UE distance (m)	Ant. conf.	Min SNR (dB)
1	4	HQSTBC	37	4	9.4
				8	9.6
		T-BF	37	4	8.2
			52	8	7.3
	5	HQSTBC	22	4	14.0
				8	14.0
		T-BF	37	4	9.6
			37	8	7.8
	7	HQSTBC	--	--	--
		T-BF	22	4	13.8
			22	8	10.2
2	4	HQSTBC	22	4	10.1
			22	8	10.5
		T-BF.	22	4	8.7
			42	8	6.6
	5	HQSTBC	22	4	12.9
			22	8	13.6
		T-BF	22	4	11.1
			22	8	8.1
	7	HQSTBC	--	--	--
		T-BF	14	4	14.5
			22	8	12.0

Table VI compares the two algorithms used in this study in the 28 GHz band, with the AP is at the end of the wagon (Scenarios 1 and 2). The table shows the maximum distance reached and the configuration with which it was achieved (see Fig. 3). It also shows the minimum SNR required to maintain the maximum throughput under the various MCS schemes. It shows that Scenario 1 offered the best performance in terms of maximum distance reached. For instance, using 8 antennas, we observed that applying the beamforming (T-BF) algorithm, distance of 52 m could be reached using the MCS 4 (3.08 Gbps) scheme. However, under the same conditions in the Scenario 2 the maximum throughput was maintained up to 42 m. This is because in the Scenario 1 at 28 GHz, according to Fig. 4,

the SNR applied at 52 m was 11 dB. Therefore, the minimum SNR is exceeded which at 52 m (MCS4) is 7.3 dB, according to Table VI. However, in the Scenario 2 the SNR applied at 52 m is lower than in the Scenario 1 not exceeding the minimum SNR needed.

Table VII shows the same parameters as Table VI, but is comparing Scenarios 3 and 4. In Scenario 3 applying the beamforming algorithm, a maximum distance of 33.5 m is reached, maintaining a throughput of 4.62 Gbps when the MCS 5 scheme is used. While applying the MCS 7 scheme, a maximum throughput of 5.77 Gbps can be reached up to a distance of 24.5 m. However, in Scenario 4, a maximum throughput of 5.77 Gbps is obtained up to a distance of 29.5 m. According to Fig. 4, Scenario 4 is more favorable in terms of SNR allowing longer distances to be reached.

2) Performance According to Algorithm

Analyzing the results obtained by applying the HQSTBC algorithm, the Table VI shows that in Scenarios 1 and 2 the minimum required SNR when applying MCS 4 and MCS 5 is larger using 8 antennas than using 4. For example, in Scenario 2 a maximum distance of 22 m is reached under MCS 4 and for this a minimum SNR of 10.1 dB with 4 antennas and 10.5 dB with 8 antennas is required. This is because, as shown in Table III, the mean correlation, calculated from H shown in (4), at 22 m using 4 and 8 antennas were 0.41 and 0.44, respectively. However, according the Table V the mean correlation, calculated from coded H shown in (5) and (6), at 22 m using 4 and 8 antennas were 0.37 and 0.29, respectively. Therefore, in this example the minimum required SNR is justified by the mean correlation obtained from the matrix H defined in (4), requiring a higher SNR when the correlation is higher.

However, in both Scenarios 3 and 4 (see Table VII), in general, the minimum required SNR is higher using 4 antennas than using 8. For example, in Scenario 4 applying MCS 4 requires a minimum SNR of 12 dB to reach 29.5 m with 4 antennas and 9.2 dB with 8 antennas. This can be explained in this case by observing the mean correlation calculated from coded H shown in (5) and (6). According to Table V these mean correlations are 0.41 and 0.21 using 4 and 8 antennas, respectively. This implies a difference between correlations of 0.2, whereas in the example above the difference is 0.08. Therefore, it can be concluded that the minimum required SNR with 4 and 8 antennas depends on the mean correlation calculated from the encoded H. However, it will depend on the mean correlation obtained from the coded H when this mean correlation presents a difference between the correlation obtained with 4 and 8 antennas higher than or equal to 0.2.

Better results were obtained with the transmit beamforming algorithm than the HQSTBC algorithm. This can be confirmed by inspecting Table VI and VII, which show that independently of the scenario, for a given number of antennas and MCS scheme, the distance

reached using the HQSTBC algorithm is always less than or equal to that reached with the beamforming algorithm. It is important to note that in the cases where the distances are identical the minimum SNR required is always higher for the HQSTBC algorithm. For instance, in Scenario 1 using 8 antennas and the MCS4/T-BF it is possible to reach up to 52 m, applying a minimum SNR of 6.7 dB to maintain a maximum throughput of 3.08 Gbps. In comparison, using MCS4/HQSTBC a distance of 37 m is achieved by applying a minimum SNR of 9.6 dB. In addition, using the HQSTBC algorithm and the MCS 7 scheme the throughput is zero at all distances. This is because it uses a 64 QAM modulation and the correlation has a strong influence on the throughput, so a higher SNR than shown in Fig. 4 is required. However, in Scenario 1, applying the beamforming algorithm in combination with MCS 7 schemes up to 22 m can be reached with both 4 and 8 antennas.

TABLE VII
MAXIMUM DISTANCE, MINIMUM SNR AND ANTENNA CONFIGURATION FOR EACH ALGORITHM FOR BOTH STANDING AND SITTING (AP IN THE MIDDLE AT 28 GHz)

Sce.	MCS	MISO algorithm	Max. train cabin - UE distance (m)	Ant.	Min SNR (dB)
3	4	HQSTBC	33.5	4	9.5
			33.5	8	9.7
		T-BF	33.5	4	9.2
			33.5	8	6.7
	5	HQSTBC	24.5	4	14
			24.5	8	9.4
		T-BF	24.5	4	11.4
			33.5	8	8.2
	7	HQSTBC	--	--	--
		T-BF	24.5	4	16.0
			24.5	8	11.5
4	4	HQSTBC	29.5	4	12.0
			29.5	8	9.2
		T-BF	29.5	4	9.4
			29.5	8	6.7
	5	HQSTBC	29.5	4	13.8
			29.5	8	11.5
		T-BF	29.5	4	11.3
			29.5	8	8.3
	7	HQSTBC	--	--	--
		T-BF	29.5	4	17.2
			29.5	8	11.3

V. CONCLUSION

This paper uses MISO-OFDM techniques to analyze transmission in an intra-wagon environment at the 28 and 37 GHz bands in terms of SNR, correlation and throughput. Four scenarios based on varying the position of the AP (end or middle wagon) and the height of the UE (standing or sitting) were analyzed. A space-time algorithm (HQSTBC) and an algorithm based on transmit beamforming with 4 and 8 antennas have been simulated. In terms of correlation, overall at 37 GHz the best performance is obtained when the AP is at the end of the wagon and the UE is standing, while when the AP is in the middle of the wagon the performance is obtained when the UE is seated. However, at 28 GHz the best

performance is obtained when the UE is standing, regardless of the AP location. The 37 GHz band is better according the correlation, while the 28 GHz band is better in terms of SNR. For this reason, the best throughput is obtained at 28 GHz using beamforming because it is not influenced by the correlation but by the SNR applied. The contrary happens with the algorithm HQSTBC, since this is an algorithm influenced by the correlation. Finally, according the throughput applying beamforming better to use 8 antennas than 4 due to array gain, since longer distances are reached even applying lower SNRs.

REFERENCES

[1] World Bank. 2017. Railway reform: Toolkit for improving rail sector performance (English). Washington, D.C.: World Bank Group. http://documents.worldbank.org/curated/en/529921469672181559/Railway-reform-Toolkit-for-improving-rail-sector-performance

[2] K. Guan, G. Li, T. Kürner, A. F. Molisch, B. Peng, R. He, B. Hui, J. Kim and Z. Zhong, "On millimeter wave and THz mobile radio channel for smart rail mobility," *IEEE Trans. Veh. Technol.*, vol. 66, pp. 5658–5674, Nov. 2016.

[3] Al-Dulaimi, X. Wang, and I. Chih-Lin, 5G Networks: Fundamentals requirements, enabling technologies, and operations management. John Wiley & Sons, 2018.

[4] K. David and H. Berndt, "6G vision and requirements: Is there any need for beyond 5G? *IEEE Veh. Technol. Mag.*, vol. 13, no. 3, pp. 72-80, Sept. 2018.

[5] T. S. Rappaport, R. W. Heath, R. C. Daniels y J. N. Murdock, Millimeter waves wireless communications. Prentice Hall. 2016.

[6] Provisional final acts (WRC-19), The World Radiocommunication Conference (Sharm el-Sheikh, 2019).

[7] M. Soliman, P. Unterhuber and D. Gera, "First analysis of inside Train communication with ITS-G5 measurement data," *2016 International Symposium on Wireless Communication Systems (ISWCS)*, Poznan, 2016, pp. 451-455.

[8] K. Li et al., "Efficient environment model for intra-wagon millimeter wave ray-tracing simulation," *2017 IEEE International Symposium on Antennas and Propagation & USNC/URSI National Radio Science Meeting*, San Diego, CA, 2017, pp. 1909-1910.

[9] C.-X. Wang, A. Ghazal, B. Ai, Y. Liu, and P. Fan, "Channel measurements and models for high-speed train communication systems: A survey", *IEEE Trans. Intell. Transp. Sys.*, vol. 18, pp. 974–987, Dec. 2017.

[10] B. Bulut, T. Barratt, D. Kong, J. Cao, A. L. Freire, F. Tila, S. Armour, M. Beach and A. Nix, "Millimeter wave channel measurements in a railway depot", in *IEEE 28th Annu. Int. Symp. Person. Indoor Mobile Radio Commun. (PIMRC)*, pp. 1–5, Montreal, Oct. 2017.

[11] D. He *et al.*, "Influence of Typical Railway Objects in a mmWave Propagation Channel," *IEEE Transactions on Vehicular Technology*, vol. 67, no. 4, pp. 2880-2892, April 2018.

[12] J. M. García-Loygorri, C. Briso, I. Arnedo, C. Calvo, M. A. G. Laso, D. He, F. Jiménez, and V. González, "Wideband channel modeling for mm-wave inside trains for 5G-related applications", *Wireless Commun. Mobile Comput.*, vol. 2018, Article ID 6916954, pp. 1–11, Apr. 2018.

[13] L. Rubio *et al.*, "Millimeter wave channel measurements in an intra-wagon environment," *IEEE Transactions on Vehicular Technology*. doi: 10.1109/TVT.2019.2947205 (In Early Access).

[14] K. Guan et al., "Channel Characterization for Intra-Wagon Communication at 60 and 300 GHz Bands," *IEEE Transactions on Vehicular Technology*, vol. 68, no. 6, pp. 5193-5207, 2019.

[15] Anoh, Kelvin, G. N. Okorafor, Bamidele Adebisi, Ali Alabdullah, Steve Jones and Raed A. Abd-Alhameed. "Full-Diversity QO-STBC Technique for Large-Antenna MIMO Systems", *Electronics*, vol. 6.2, no. 37, May 2017.

[16] C. Sanchis, M.T. Martinez, J.M. Molina, J. Pascual and J.V. Rodriguez, "Experimental Study of MIMO-OFDM Transmissions at 94 GHz in Indoor Environments," *IEEE Access*, vol. 5, 7488-7494, Apr. 2017.

[17] Ju-Hong Lee and Wei-En Sun, "Robust beamforming and spatial precoding for quasi-OSTBC massive MIMO communications ", *EURASIP Journal on Wireless Communications and Networking.* vol. 58, pp. 1-16, 2019.

[18] T. Lin, J. Cong, Y. Zhu, J. Zhang, and K. B. Letaief, "Hybrid beamforming for millimeter wave systems using the MMSE criterion," *IEEE Trans. Commun.*, vol. 67, no. 5, pp. 3693-3708, 2019.

[19] Thomas Kaiser, "Smart Antennas: State of the Art," Hindawi Publishing Corporation, 2005.

[20] D. Shiu, G. J. Foschini, M. J. Gans and J. M. Kahn, "Fading correlation and its effect on the capacity of multielement antenna systems," *IEEE Transactions on communications*, vol. 48, pp. 502-513, 2000.

[21] M. Yusuf, E. Tanghe, M.T. Martinez, J. Pascual, J.M. Molina, L. Martens and W. Joseph, "Frequency-Dependence Characterization of Electromagnetic Reverberation in Indoor Scenarios Based on 1–40 GHz Channel Measurements", *IEEE Antennas and Wireless Propagation Letters*, vol. 18, no. 10, pp. 2175-2179, 2019.

[22] A. F. Molisch, *Wireless communications*, 2nd ed. Wiley-IEEE Press, 2010.

[23] R. Steele and L. Hanzo, *Mobile radio communications*, 2nd Ed. Wiley, 1999.

[24] Wireless Medium Access Control (MAC) and Physical Layer (PHY) Specifications for High Rate Wireless Personal Area Networks (WPANs) Amendment 2: Millimeter-wave-based Alternative Physical Layer Extension, IEEE 802.15.3, 2009.

[25] D.P. McNamara, M.A. Beach and P.N. Fletcher, "Spatial Correlation in Indoor MIMO Channels", *IEEE International Symposium on Personal, Indoor and Mobile Radio Communications*, 2002.

[26] M. Martinez-Ingles, C. Sanchis-Borras, J. Molina-Garcia-Pardo, J. Rodríguez and L. Juan-Llácer, "Experimental Evaluation of an Indoor MIMO-OFDM System at 60 GHz Based on the IEEE802.15.3c Standard," *IEEE Antennas and Wireless Propagation Letters*, vol. 12, pp. 1562-1565, 2013.